Giant low frequency dielectric tunability in high-*k* $Ba(Fe_{1/2}Nb_{1/2})O_3$ ceramics at room temperature

Shanming Ke and Haitao Huang[a)]
Department of Applied Physics and Materials Research Center, The Hong Kong Polytechnic University, Hung Hom, Kowloon, Hong Kong

(Received 11 June 2010; accepted 7 August 2010; published online 17 September 2010)

The effect of electric field on the dielectric properties of high-*k* $Ba(Fe_{1/2}Nb_{1/2})O_3$ ceramics with different grain sizes is reported. A low frequency giant dielectric tunability (>85%) can be obtained under a bias field as low as 50 V/mm. The results suggest that the giant dielectric tunability originates from extrinsic contributions such as domain boundary and oxygen defect relaxations. These findings provide a clear understanding to the complicated dielectric response in a family of high-*k* ceramics and a key to the high tunability of nonferroelectrics under low electric fields, which is attractive for potential applications in tunable devices. © *2010 American Institute of Physics*. [doi:10.1063/1.3487472]

I. INTRODUCTION

Fe-containing double perovskites in the general form $A(Fe_{1/2}B_{1/2})O_3$ (A=Ba, Sr, Ca; and B=Nb, Ta, etc., shorted as AFN hereafter) have been actively investigated in order to understand the nature of magnetism and magnetotransport in these compounds.[1,2] Similar to the high permittivity observed in $CaCu_3Ti_4O_{12}$ (CCTO),[3] these AFN oxides were reported to have a giant dielectric constant ($>10^4$) and show weak temperature dependence over a wide temperature range of 100–400 K.[4–13] It has been clarified that unlike $Pb(Fe_{1/2}B_{1/2})O_3$ (B=Nb, Ta), AFN shows no ferroelectricity. However, there are two typical dielectric relaxations in AFN ceramics, a Debye-type relaxation at low temperatures (50–300 K) and a relaxorlike relaxation with strong frequency dispersion at relatively high temperatures (400–700 K).[4–6] The former relaxation can be explained by a polaronlike model and the latter can be attributed to the oxygen defect induced dielectric anomaly.[4,9]

$Ba(Fe_{1/2}Nb_{1/2})O_3$ (BFN) is antiferromagnetic with a weak ferromagnetic behavior at 5 K.[1,2] Sinha *et al.*[10,11] attributed the giant dielectric response to a ferroelectric relaxor nature in BFN. However, first-principles calculations show that BFN is not a ferroelectric.[12] Instead, BFN is a cubic (a =0.4045 nm, space group *Pm*3*m*) or a monoclinic perovskite depending on the sintering conditions.[4–12] Compared to the intensively investigated CCTO, which has similar dielectric properties, BFN is much less investigated, especially on its microstructure.

In our precious studies, a B-site precursor ("columbite") method, using $FeNbO_4$ precursor, has been proved to be an optimal process to synthesize BFN with no secondary phases[5,6] and the grain growth could be suppressed effectively. In this work, we report the dielectric response of BFN ceramics under a dc bias field. The dielectric response and the ac conductivity are strongly dependant on the microstructure which is determined by the fabrication conditions. A large dielectric tunability in BFN compounds can be obtained with a dc bias field as low as 50 V/mm.

II. EXPERIMENTAL

To study the effect of microstructure on the dielectric properties, two types of BFN with different microstructures were synthesized. One type of samples was named BFN-C which was synthesized by the "columbite" method. In this method, $FeNbO_4$ (FN) precursor with a monoclinic phase[5] was first synthesized by a solid-state reaction of reagent grade iron oxide, Fe_2O_3, and niobium oxide, Nb_2O_5, at 1075 °C. Powders of FN were then mixed with $BaCO_3$ and ball milled in ethyl alcohol for 12 h followed by calcination at 1200 °C for 8 h. The calcined BFN powders were then compacted into green pellets by cold isostatic pressing and sintered in air at 1300 °C for 6 h. Another type of samples was called BFN-M which was synthesized by a direct mixed oxide method. In this method, reagent grade iron oxide (Fe_2O_3), barium carbonate ($BaCO_3$), and niobium oxide (Nb_2O_5) were directly mixed and ball milled. The mixture was dried and calcined and finally sintered in air at 1300 °C.

The phase and microstructure of synthesized BFN ceramics were examined by x-ray diffraction and scanning electron microscope (SEM, Leica Stereoscan 440), respectively. The results were reported elsewhere.[5,6] For dielectric measurement, the electrodes were made by coating silver paint on both surfaces of the sintered disks and fired at 650 °C for 20 min. The sample pellets were 10 mm in diameter and about 1 mm in thickness. The dielectric properties were measured by using a frequency-response analyzer (Novocontrol Alpha-analyzer) over a broad frequency range (0.1 Hz–10 MHz) at various temperatures down to −120 °C.

III. RESULTS AND DISCUSSION

A. Large low frequency tunability in BFN

Figure 1 shows the temperature dependence of the real part of dielectric constant (ε') of BFN-C measured at 100 Hz under a zero bias electric field in air. The dielectric constant

a)Electronic mail: aphhuang@polyu.edu.hk.

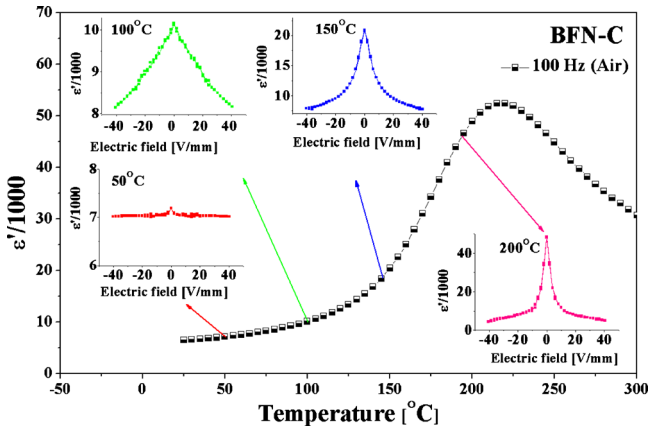

FIG. 1. (Color online) Temperature dependence of the real part of the dielectric constant of BFN-C ceramics measured at 100 Hz. The insets show the dielectric constant as a function of dc bias electric field at selected temperatures.

ε' exhibits a giant value and a broad peak at the temperature (T_{max}) around 220 °C. The four insets in Fig. 1 are the plots of the dielectric constant against applied dc bias field at selected temperatures. The value of ε' decreases with increasing bias field at above 50 °C, while it remains nearly constant with bias field at below 50 °C for BFN-C. Compared to ferroelectric materials, BFN-C exhibits quite a different *C-V* behavior; its dielectric constant varies nonlinearly with an applied voltage without a hysteresis.

The *C-V* behavior of BFN-M is similar to that of BFN-C. Most importantly, as presented in Fig. 2(a), a large variation in dielectric constant with applied voltage at 100 Hz has been observed in BFN-M at room temperature. Figure 2(b) displays the temperature dependence of ε' and loss tangent (tan δ) of BFN-M at 100 Hz without a bias field. It is noted that ε' of BFN-M exhibits a giant value and a broad peak appears at the temperature (T_{max}) close to that of BFN-C. It should be emphasized that $\varepsilon'(T)$ of BFN-M shows a shoulder around room temperature which is accompanied by a tan δ peak, while both $\varepsilon'(T)$ and tan $\delta(T)$ of BFN-C increase monotonically in the same temperature range.

The relative tunability as a function of dc bias field of BFN-C and BFN-M at selected temperatures and/or frequencies is shown in Fig. 3. Here, the relative tunability n_r is

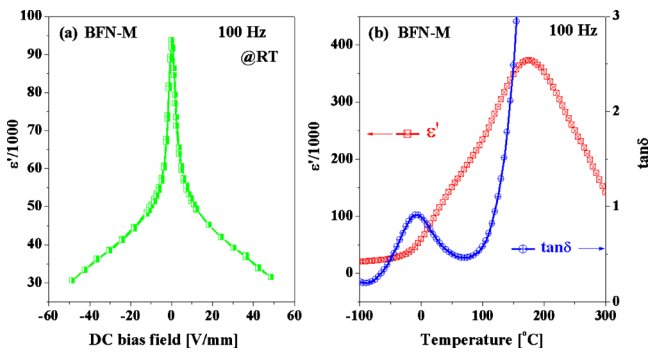

FIG. 2. (Color online) (a) The real part of the dielectric constant of BFN-M as a function of dc bias electric field at room temperature. (b) Temperature dependence of the dielectric constant and loss tangent of BFN-M ceramics measured at 100 Hz.

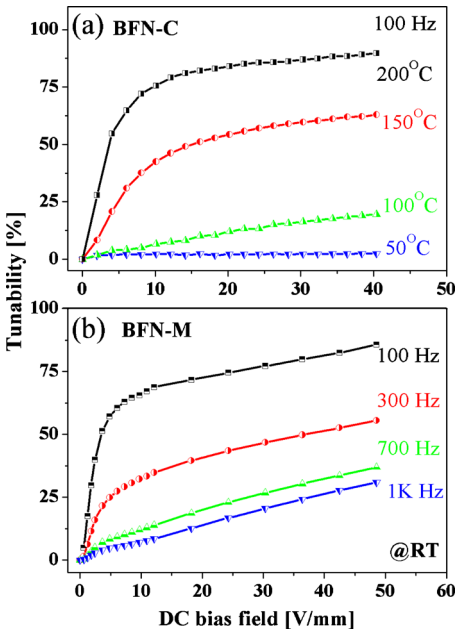

FIG. 3. (Color online) Relative tunability as a function of dc bias field (a) for BFN-C measured at different temperatures under 100 Hz and (b) for BFN-M measured under different frequencies at room temperature.

defined as $n_r=[\varepsilon(0)-\varepsilon(E)]/\varepsilon(0)$, where $\varepsilon(0)$ and $\varepsilon(E)$ represent the dielectric constants under a bias field of zero and E, respectively. It can be seen that the tunability increases with increasing dc fields and a large tunability can only be achieved in a relatively high temperature range close to T_{max} of BFN-C. However, a giant tunability over 85% under a bias field of 50 V/mm in BFN-M at 100 Hz could be observed at room temperature. At a fixed electric field, the tunability of BFN-M decreases with increasing frequencies as shown in Fig. 3(b).

Since tunability is a measure of the electric field dependence of the dielectric constant, it is necessary to list all possible polarization mechanisms which contribute to the dielectric constant of a material. Generally, there are seven kinds of polarization mechanisms as follows:[13,14] (1) intrinsic polarization of ferroelectric polar-regions (domains); (2) thermal fluctuation of spontaneous polarization of polar nanoregions; (3) domain wall motion; (4) boundary motion between ferroelectric and paraelectric nanoregions; (5) intrinsic polarization of paraelectric phase; (6) polarization of defect dipoles; and (7) polarization contribution of inhomogeneous conduction [Maxwell–Wagner (M–W) relaxation]. Among them, mechanisms (1)–(4) are specifically assigned to ferroelectric materials. The intrinsic polarization of a paraelectric material usually makes a constant contribution to the dielectric constant up to a high frequency under a small dc bias field (such as 50 V/mm). So the large tunability observed in BFN-C and BFN-M should be resulted from mechanism (6) and/or (7).

B. Dielectric response of BFN-C above room temperature

M–W relaxation can occur in samples with a variety of heterogeneities, such as, the depletion layer between the

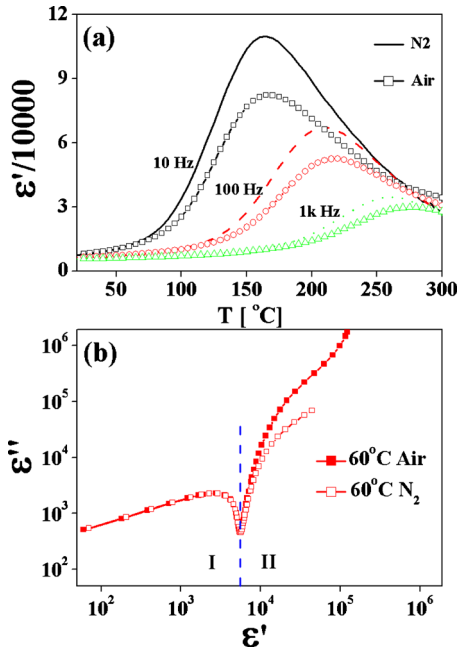

FIG. 4. (Color online) (a) The temperature dependences of the dielectric constant at various frequencies for BFN-C measured in flowing N_2 and air, respectively. (b) Cole–Cole plot for the dielectric constant of BFN-C at 60 °C.

sample and electrode, and the interfacial layer at grain boundary and/or domain boundary. The capacitance of a depletion layer is strongly influenced by an applied bias voltage according to

$$C = \sqrt{e\varepsilon' N_d/2(V_d + V)}, \tag{1}$$

where V_d is the diffusion potential and N_d is the concentration of donors.[15] Because the capacitances of BFN-C and BFN-M shown in Figs. 1 and 2 did not follow this relation (except at very low voltage), it is concluded that the large tunability observed in BFN-C is unlikely to be resulted from depletion layer formed between the sample surface and the electrode.

The insulating grain boundary and/or domain boundary with semiconducting grains (i.e., internal barrier layer capacitance mechanism, IBLC) may lead to giant dielectric response that can be tuned by applied dc bias fields. However, this IBLC mechanism in BFN-C can also be excluded. A close examination in Fig. 1 shows that, by applying an electric field of about 40 V/mm, the dielectric constant of BFN-C could be suppressed to a plateau value ~7000 within the whole temperature range of measurement. This means the tunability observed in BFN-C is strongly related to the dielectric peak around T_{max}. However, from the equivalent circuit simulation, IBLC mechanism itself could not yields such a dielectric peak. Therefore, the large tunability in BFN-C at above room temperature mainly comes from mechanism (6), i.e., polarization of normal defect dipoles.

Figure 4(a) shows the temperature dependences of the real part of dielectric constant for BFN-C at various measuring frequencies in flowing air and N_2, respectively. It can be seen that T_{max} is frequency dependent and it shifts to higher temperatures with increasing frequencies showing a relaxor-

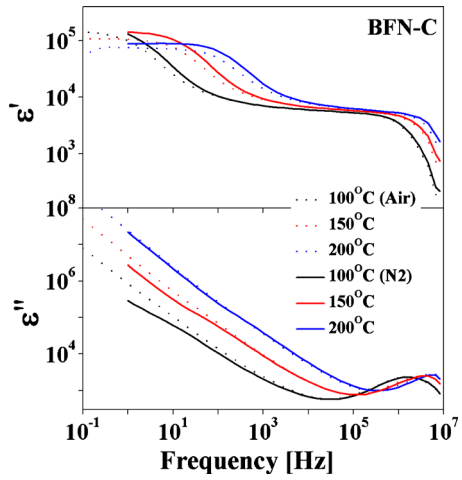

FIG. 5. (Color online) Frequency dependences of (a) the real part and (b) the imaginary part of the complex dielectric constant at various frequencies for BFN-C measured in flowing N_2 and air, respectively.

like behavior. However, the frequency dispersion is much stronger than that in typical relaxor ferroelectrics such as $Pb(Mg_{1/3}Nb_{2/3})O_3$ (PMN). The difference (ΔT_{max}) between T_{max} at 1 kHz and that at 10 Hz for BFN-C is greater than 150 K while that for PMN is just 12 K.

Chen *et al.*[4] found that the dielectric peak of BFN could be greatly suppressed by annealing the sample in oxygen. Here in our BFN-C sample, the dielectric peak is greatly enhanced by measuring in flowing N_2, i.e., the maximum dielectric constant is increased from 82 300 in air to over 109 800 in N_2 when measured under 10 Hz, as shown in Fig. 4. This result again strongly implies that the dielectric peaks are closely related to oxygen vacancies.

Putting together the above analysis, the large tunability of BFN-C shown in Fig. 3(a) can be attributed to the field dependent polarization of defect dipoles that are associated with oxygen vacancies. The complex plane plots of ε'' versus ε' measured at 60 °C under N_2 and air, respectively, are shown in Fig. 4(b). Two easily distinguishable contributions can be identified as follows: region I (at high frequency) and region II (at low frequency). In region I, the relatively small semicircle originates from the polaron relaxation effect and is not influenced by the measuring atmosphere. Region II, however, is sensitive to the measuring atmosphere and is related to the oxygen defect dipoles.

Further evidence for oxygen defect induced dielectric peaks and large tunability in BFN can be found from the frequency dependences of the complex dielectric constant $\varepsilon'(f)$ and $\varepsilon''(f)$ for a series of temperatures, as shown in Fig. 5. In the high frequency regime (>100 kHz), the $\varepsilon''(f)$ curves begin to merge and form a peak above 1 MHz, which is accompanied by a steplike decrease in $\varepsilon'(f)$. This Debye-like relaxation is attributed to a polaron relaxation process. In the low frequency regime (<1 kHz), a steplike decrease in $\varepsilon'(f)$ similar to that in the high frequency regime can be found. However, $\varepsilon''(f)$ displays a linear relationship with frequency, which is a common feature in a system dominated by dc conductivity.[16] By excluding the contribution of dc conductivity using

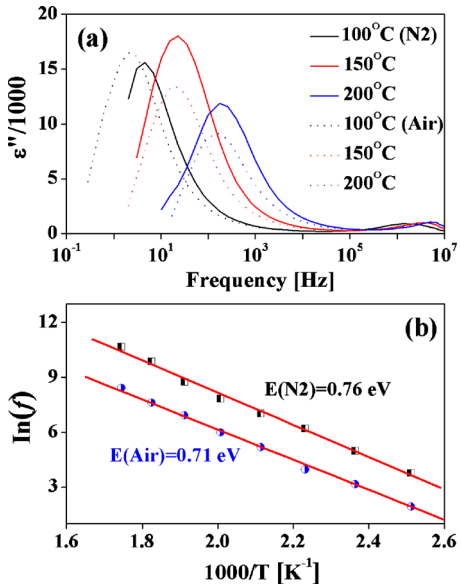

FIG. 6. (Color online) (a) Imaginary part of the dielectric constant of BFN-C after subtracting the contribution from dc conductivity using Eq. (2). (b) Arrhenius plot according to Eq. (3).

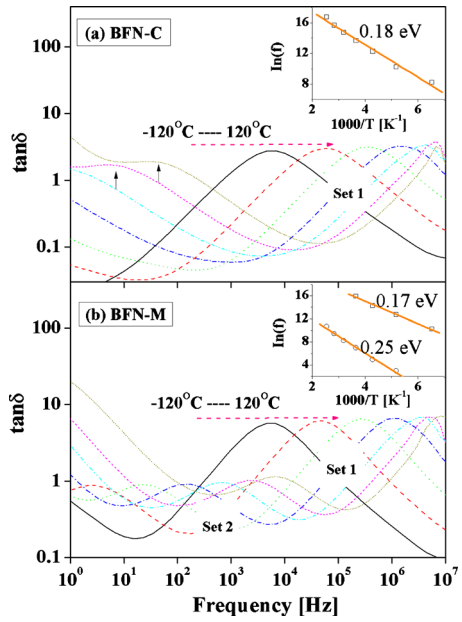

FIG. 7. (Color online) Frequency dependence of the loss tangent at various temperatures for (a) BFN-C and (b) BFN-M measured in flowing air. The insets show the Arrhenius plots according to Eq. (3).

$$\varepsilon''(f) = [\sigma'(f) - \sigma_{dc}]/\omega, \tag{2}$$

the imaginary part of dielectric constant arising from pure dipole polarization can be obtained. Figure 6(a) plots such $\varepsilon''(f)$ curves calculated from Eq. (2). As expected, $\varepsilon''(f)$ peaks reappear in the low frequency regime and they shift to higher frequencies with increasing temperatures. The activation energies for the low frequency relaxation processes can be calculated by using an Arrhenius relation,

$$f = f_0 \exp(-E/k_B T), \tag{3}$$

where E is the activation energy and k_B is the Boltzmann constant. They are 0.76 and 0.71 eV in N_2 and air, respectively, which are very close to the value of the energy barrier for $V_O^{\bullet\bullet}$ in perovskites.

C. Domain boundary effect in BFN-M

It has been mentioned that the high temperature dielectric relaxation in BFN-M is similar to that in BFN-C, where a large tunability can be found around the dielectric relaxation peaks (50–300 °C). However, another giant tunability in BFN-M is observed also at around room temperature [Fig. 3(b)], which is accompanied by a dielectric relaxation around the same temperature [Fig. 2(b)]. This behavior is not observed in BFN-C.

To clarify this dielectric relaxation process and the large tunability observed at room temperature in BFN-M, the frequency dependences of the loss tangent (tan δ) of BFN-C and BFN-M are plotted in Fig. 7. Two types of relaxation process, i.e., set 1 for high frequency relaxation and set 2 for low frequency relaxation, can be easily distinguished in BFN-M. Both sets of relaxation peaks shift to higher frequencies with increasing temperatures. For BFN-C, the relaxation in the high frequency region is very similar to that of BFN-M. However, in the low frequency region, as indicated by arrows, the relaxation peak is too weak to be observed. By using Eq. (3), the activation energies for the high frequency relaxation are 0.18 and 0.17 eV for BFN-C and BFN-M, respectively, which are very close to the reported value of 0.174 eV for BFN ceramics.[4] The activation energy for the low frequency relaxation is 0.25 eV for BFN-M.

To further explore the dielectric responses in BFN, the electric modulus (reciprocal of dielectric constant) and the corresponding Arrhenius plot were shown in Fig. 8. The electric modulus formalism now is often used together with impedance and permittivity formalisms to separate the grain and grain boundary effects.[17] Two and three sets of frequency responses were observed in BFN-C and BFN-M, respectively. The corresponding activation energies calculated were 0.16 and 0.53 eV for BFN-C, and 0.15, 0.24, and 0.39 eV for BFN-M. Similar to CCTO, usually, three sets of relaxation peaks will be observed which can be ascribed to the contributions from grains, grain boundaries, and domain boundaries. Here, the two sets of relaxation in BFN-C were contributed by grains and grain boundaries. The additional set of relaxation observed in BFN-M [set 2 in Fig. 7(b)] can be attributed to the domain boundary effect. Since the room temperature tunability of BFN-C is relatively small, the extra large tunability of BFN-M at room temperature can be ascribed to the dielectric response of domain boundaries.

Figure 9 shows the variation in ac conductivity σ with frequency at various temperatures for BFN ceramics. For BFN-C, the conductivity σ shows a rapid increase at low frequencies, which is due to the blocking effect of grain boundaries. At high frequencies, it increases slowly with frequency, which is dominated by a variable-range-hopping mechanism. For BFN-M, there is another rapid increase [indicated by a dashed in Fig. 9(b)] located in the low frequency range.

It is well known that the ac conductivity due to localized states in a material can be described by

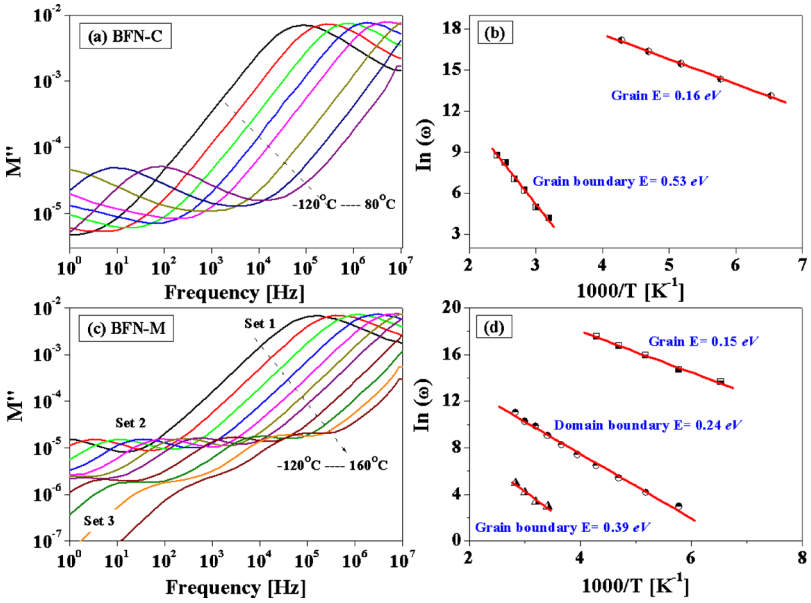

FIG. 8. (Color online) Electric modulus as a function of frequency at various temperatures for (a) BFN-C and (c) BFN-M. (b) and (d) are the corresponding Arrhenius plots according to Eq. (3).

$$\sigma' = \sigma_{dc} + Af^n, \tag{4}$$

where $0<n<1$, σ_{dc} is the dc conductivity, and A is a constant. This is a universal power law and corresponds to the short range hopping of charged particles through trapped sites separated by energy barriers of varied heights. If a single charged particle moves across multiple barrier heights, the conductivity will show multiple steep increases as a function of frequency (following the above equation).[18] There are two kinds of insulating barriers present in BFN ceramics that can cause such a frequency dependence of conductivity; domain boundaries and grain boundaries. In BFN-M, the rapid increase in conductivity in the high frequency region is due to the blocking effect of grain boundaries, similar to that observed in BFN-C (Fig. 9). The rapid increase in conductivity in the low frequency region, as indicated by the dashed line in Fig. 9(b), is due to the blocking effect of domain boundaries in BFN-M. The reason that the domain boundary blocking effect is too weak to be observed in BFN-C is related to its microstructure. From the SEM images (Fig. 10) of both types of samples, it can be seen that, as compared to BFN-M, BFN-C has a much smaller grain size and hence results in much less domain boundaries. Similar relation between the quantity of domain boundaries and grain size is also reported in CCTO.[19,20]

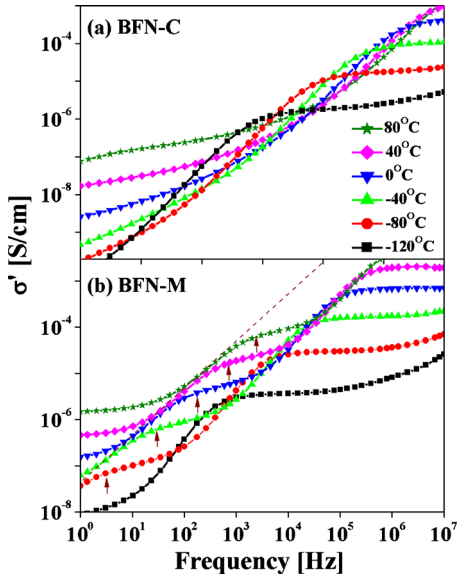

FIG. 9. (Color online) Frequency dependent ac conductivity at various temperatures for (a) BFN-C and (b) BFN-M. The arrows indicate the peak frequencies shown in Fig. 7. The dashed line is a guide to the eye showing the rapid increase in conductivity with increasing frequency following Eq. (4).

IV. CONCLUSION

In conclusion, BFN ceramics with different grain size were fabricated by a columbite method (BFN-C) and a mixed oxide solid state method (BFN-M). Both samples reveal broad relaxorlike dielectric peaks and a giant tunability round this peak, which were originated from the polarization

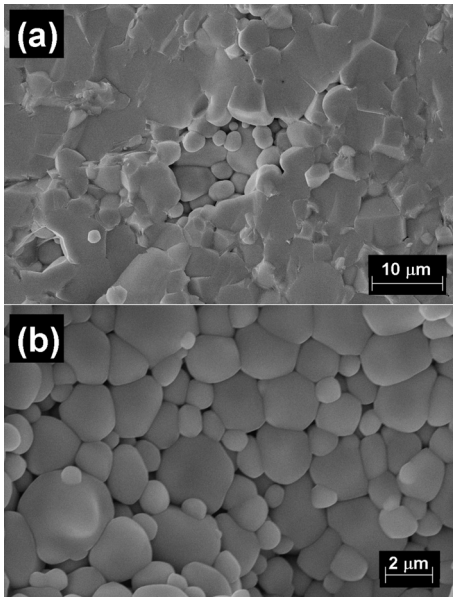

FIG. 10. Typical SEM images of (a) BFN-M and (b) BFN-C.

of oxygen defect dipoles. At room temperature, the tunability of BFN-C was relatively small. However, a giant tunability of over 85% was observed in BFN-M under a bias field of 50 V/mm at room temperature. This was attributed to the domain boundary effect, which was not observed in BFN-C with only a small amount of domain boundaries.

ACKNOWLEDGMENTS

This work was supported by the Research Grants Council of the Hong Kong Special Administrative Region, China (Project No.: PolyU 5171/07E) and Hong Kong Polytechnic University (Projects: A-SA11 and A-PJ46).

[1]K. Tezuka, K. Henmi, Y. Hinatsu, and N. M. Masaki, J. Solid State Chem. **154**, 591 (2000).
[2]N. Rama, J. B. Philipp, M. Opel, K. Chandrasekaran, V. Sankaranarayanan, R. Gross, and M. S. R. Rao, J. Appl. Phys. **95**, 7528 (2004).
[3]S. Ke, H. Huang, and H. Fan, Appl. Phys. Lett. **89**, 182904 (2006).
[4]Z. Wang, X. M. Chen, L. Ni, and X. Q. Liu, Appl. Phys. Lett. **90**, 022904 (2007).
[5]S. Ke, H. Huang, H. Fan, H. L. W. Chan, and L. M. Zhou, Ceram. Int. **34**, 1059 (2008).
[6]S. Ke, H. Fan, and H. Huang, J. Electroceram. **22**, 252 (2009).
[7]N. Charoenthai, R. Traiphol, and G. Rujijanagul, Mater. Lett. **62**, 4446 (2008).
[8]C. Chung, Y. Chang, and G. Chen, J. Appl. Phys. **96**, 6624 (2004).
[9]I. P. Raevski, S. A. Kuropatkina, S. P. Kubrin, S. I. Raevskaya, V. V. Titov, D. A. Sarychev, M. A. Malitskaya, A. S. Bogatin, and I. N. Zakharchenko, Ferroelectrics **379**, 48 (2009).
[10]S. Saha and T. P. Sinha, Phys. Rev. B **65**, 134103 (2002).
[11]S. Saha and T. P. Sinha, J. Phys.: Condens. Matter **14**, 249 (2002).
[12]R. Demirbilek, A. I. Gubaev, A. B. Kutsenko, S. E. Kapphan, I. P. Raevski, S. A. Prosandeev, B. Burton, L. Jastrabik, and V. S. Vikhnin, Ferroelectrics **302**, 279 (2004).
[13]X. Y. Wei and X. Yao, Int. J. Mod. Phys. B **20**, 2977 (2006).
[14]G. A. Smolensky, J. Phys. Soc. Jpn. **28**, 26 (1970).
[15]J. Yu, T. Ishikawa, Y. Arai, S. Yoda, M. Itoh, and Y. Saita, Appl. Phys. Lett. **87**, 252904 (2005).
[16]P. Lunkenheimer, V. Bobnar, A. V. Pronin, A. I. Ritus, A. A. Volkov, and A. Loidl, Phys. Rev. B **66**, 052105 (2002).
[17]J. Liu, C. Duan, W. Yin, W. Mei, R. W. Smith, and J. R. Hardy, Phys. Rev. B **70**, 144106 (2004).
[18]E. Barsoukov and J. R. Macdonald, *Impedance Spectroscopy Theory, Experiment, and Applications* (Wiley, New York, 2005).
[19]S. Y. Chung, I. D. Kim, and S. Kang, Nature Mater. **3**, 774 (2004).
[20]S. Y. Chung, Appl. Phys. Lett. **87**, 052901 (2005).